The Astrophysical Journal, 940:131 (13pp), 2022 December 1 https://doi.org/10.3847/1538-4357/ac9b0f

Intermediate-mass Black Holes on the Run from Young Star Clusters

Elena González Prieto[1], Kyle Kremer[2,3], Giacomo Fragione[1], Miguel A. S. Martinez[1], Newlin C. Weatherford[1], Michael Zevin[4,5], and Frederic A. Rasio[1]
[1] Center for Interdisciplinary Exploration & Research in Astrophysics (CIERA) and Department of Physics & Astronomy, Northwestern University, Evanston, IL 60208, USA; elena.prieto@northwestern.edu
[2] TAPIR, California Institute of Technology, Pasadena, CA 91125, USA
[3] The Observatories of the Carnegie Institution for Science, Pasadena, CA 91101, USA
[4] Kavli Institute for Cosmological Physics, The University of Chicago, 5640 South Ellis Avenue, Chicago, IL 60637, USA
[5] Enrico Fermi Institute, The University of Chicago, 933 East 56th Street, Chicago, IL 60637, USA
Received 2022 August 15; revised 2022 October 10; accepted 2022 October 12; published 2022 November 29

Abstract

The existence of black holes (BHs) with masses in the range between stellar remnants and supermassive BHs has only recently become unambiguously established. GW190521, a gravitational wave signal detected by the LIGO/Virgo Collaboration, provides the first direct evidence for the existence of such intermediate-mass BHs (IMBHs). This event sparked and continues to fuel discussion on the possible formation channels for such massive BHs. As the detection revealed, IMBHs can form via binary mergers of BHs in the "upper mass gap" ($\approx$40–120 $M_\odot$). Alternatively, IMBHs may form via the collapse of a very massive star formed through stellar collisions and mergers in dense star clusters. In this study, we explore the formation of IMBHs with masses between 120 and 500 $M_\odot$ in young, massive star clusters using state-of-the-art Cluster Monte Carlo models. We examine the evolution of IMBHs throughout their dynamical lifetimes, ending with their ejection from the parent cluster due to gravitational radiation recoil from BH mergers, or dynamical recoil kicks from few-body scattering encounters. We find that *all* of the IMBHs in our models are ejected from the host cluster within the first $\sim$500 Myr, indicating a low retention probability of IMBHs in this mass range for globular clusters today. We estimate the peak IMBH merger rate to be $\mathcal{R} \approx 2\ \mathrm{Gpc}^{-3}\ \mathrm{yr}^{-1}$ at redshift $z \approx 2$.

Key words: Black holes – Young star clusters – Intermediate-mass black holes – Stellar mergers – N-body simulations – Binary stars

1. Introduction

The first binary black hole (BBH) detection in 2015 (Abbott et al. 2016) revolutionized the field of gravitational wave (GW) physics. Since then, the growing catalog of GW events has sparked debates about the environments that produce these sources (e.g., The LIGO Scientific Collaboration et al. 2021a, 2021b; Abbott et al. 2020). Several features of these detections challenge our current understanding of stellar evolution and BH formation (e.g., The LIGO Scientific Collaboration et al. 2021c). An example of this is GW190521 (Abbott et al. 2021), a BBH merger with a remnant mass of $\sim$150 $M_\odot$ whose component masses both exceed the range expected from standard isolated stellar evolution. This event represents the first *direct* detection of an intermediate-mass BH (IMBH). As the number of GW detections grows and second-generation detectors such as the Laser Interferometer Space Antenna (LISA) come online, detailed stellar evolution models for massive stars are essential to our understanding of the observed BH population.

The evolutionary stages of massive stars, the progenitors of compact objects such as BHs, are expected to leave strong features on the BH mass spectrum. Massive stars with core masses between roughly 64 and 135 $M_\odot$ ($150 \lesssim M_{\rm ZAMS}/M_\odot \lesssim 260$ at $Z \sim 0.1\ Z_\odot$) undergo pair-instability supernovae (PISNe), which completely destroy the star, leaving no remnant behind (e.g., Fowler & Hoyle 1964; Ober et al. 1983; Bond et al. 1984; Belczynski et al. 2016; Woosley 2017, 2019). At lower core masses, between 32 and 64 $M_\odot$ ($70 \lesssim M_{\rm ZAMS}/M_\odot \lesssim 150$), pulsational pair-instability supernovae (PPISNe) induce severe mass-loss episodes, which limit the remnant mass (e.g., Heger & Woosley 2002). These processes should produce an "upper mass gap" in the BH mass distribution in the range $M \approx$ 40–120 $M_\odot$ (e.g., Spera & Mapelli 2017; Limongi & Chieffi 2018; Takahashi et al. 2018; Stevenson et al. 2019; Marchant et al. 2019; Farmer et al. 2019; Mapelli et al. 2020; Renzo et al. 2020; Belczynski et al. 2020). The exact boundaries of this gap are highly uncertain, with recent studies showing that the uncertainty on the carbon reaction rate can shift the lower boundary to $\sim$90 $M_\odot$ (Farmer et al. 2020; Costa et al. 2021); in this case, pair-instability-gap BBH mergers like GW190521 may be feasible through isolated binary evolution (Belczynski 2020). A second prominent feature expected from these evolutionary processes is a slight excess of BHs with masses in the range 30–40 $M_\odot$ (Stevenson et al. 2019). In its latest observing run, the LIGO–Virgo–Kagra (LVK) Collaboration reports a significant overdensity of BHs at $M \approx 30\ M_\odot$ (The LIGO Scientific Collaboration et al. 2021d).

Several formation channels for BHs in the upper mass gap have been discussed, including hierarchical mergers of lower-mass BHs (e.g., Miller & Hamilton 2002; McKernan et al. 2012; Rodriguez et al. 2018, 2019; Antonini et al. 2019; Gerosa & Berti 2019; Fragione et al. 2020, 2022; Fragione & Silk 2020; Zevin & Holz 2022), stellar mergers in dense star clusters (e.g., Portegies Zwart & McMillan 2002; Di Carlo et al. 2019; Rizzuto et al. 2021; Kremer et al. 2020a; Banerjee 2021, 2022; Banerjee et al. 2020; Weatherford et al.

2021; González et al. 2021), BH growth through gas accretion in star-forming environments (e.g., Roupas & Kazanas 2019), BH formation through gravitational instabilities in the early universe (e.g., Loeb & Rasio 1994; Carr et al. 2016), remnants of Population III stars (e.g., Madau & Rees 2001; Bromm & Larson 2004), BH–star collisions in dense star clusters (Giersz et al. 2015; Rizzuto et al. 2022), and IMBH formation from BH–star collisions in galactic nuclei (e.g., Rose et al. 2022).

In this paper we explore the formation of "low-mass" IMBHs with masses between 120 and 500 $M_\odot$. This covers the lower range of IMBH masses (typically defined as 10^2–10^5 $M_\odot$). We explore the formation of these IMBHs through repeated stellar collisions. Two distinct paths exist within this scenario, the first involving collisions between main-sequence stars and evolved stars that have a small enough core to avoid the pair instability. Spera et al. (2019) suggest that such a merger produces a star with the same initial core as the giant, but with an oversized hydrogen envelope. This merger remnant could avoid the regime where pair instability occurs in the core and collapse into a BH more massive than those formed through single-star evolution. The second path produces an IMBH via the collapse of a progenitor whose core is above the pair-instability threshold due to multiple previous massive giant collisions, as seen in Kremer et al. (2020a). We consider the general repeated stellar collisions channel described above, as well as IMBHs resulting from BBH mergers. In contrast with previous work on the formation of very massive stars ($M > 1000\,M_\odot$) in the classic collisional runaway scenario (e.g., Portegies Zwart et al. 2004; Gurkan et al. 2006; Giersz et al. 2015; Mapelli 2016), the progenitors of our IMBHs are products of only a few collisions, and thus more than one IMBH may form in a cluster at a time. Our study is limited to IMBHs with $M < 500\,M_\odot$ because treatment of such massive stars/BHs would require physics beyond what is currently implemented in CMC (e.g., loss cone physics; Umbreit et al. 2012).

In studies of young massive clusters (YMCs) with $N \approx 10^3$, Di Carlo et al. (2019) showed that BHs with masses up to $\sim 120\,M_\odot$ may form through BBH mergers but are unlikely to be retained in their host cluster. In a later study with $N \approx 10^4$, Di Carlo et al. (2021) showed that repeated stellar collisions can produce stars massive enough to directly collapse into IMBHs. In our simulations of globular cluster (GC) progenitors with $N \approx 10^5$, IMBHs also form through repeated stellar collisions, thus hinting that IMBH formation in star clusters requires massive and highly dense stellar systems, where multiple consecutive stellar collisions are common (González et al. 2021; Kremer et al. 2020a).

The exact properties of massive-star merger products remain highly uncertain, but progress is ongoing. Notably, Costa et al. (2022) and Ballone et al. (2022) recently used hydrodynamic simulations to model the mass loss and chemical composition of stellar collision products. Evolving the collision products using the stellar evolution codes Parsec and MESA, they showed that the collision products can indeed avoid pair instability and collapse into BHs in the upper mass gap. We note, however, that these studies were limited to specific collision scenarios and further study is necessary to determine if this outcome can be generalized to different masses and stellar types.

The paper is organized as follows. In Section 2, we detail the cluster modeling methodology. In Sections 3 and 4 we examine IMBH formation and evolution in the models, including an analysis of IMBH binary properties. We also explore in detail the mechanisms of IMBH ejection from the cluster and BBH mergers in Sections 5 and 6, respectively. Finally, we conclude in Section 7 with a discussion of the implications and uncertainties in our analysis.

2. Methods

We perform numerical simulations using CMC (for Cluster Monte Carlo), a Hénon-type Monte Carlo code that models the evolution of stellar clusters (Pattabiraman et al. 2013; Kremer et al. 2020b; Rodriguez et al. 2022, for the most recent review). This code incorporates prescriptions for various physical processes including two-body relaxation (Joshi et al. 2000), stellar/binary evolution using the population synthesis code COSMIC (Breivik et al. 2020), direct integration of small-N strong encounters using Fewbody (Fregeau & Rasio 2007), and stellar collisions (Fregeau & Rasio 2007).

The present study is based on the set of models listed in Table 1. All models consist of 8×10^5 objects, corresponding to an initial total cluster mass of $\approx 5 \times 10^5\,M_\odot$. The metallicity is set to 0.002 ($0.1\,Z_\odot$), and the initial conditions are King models with concentration parameter $W_0 = 5$. Stellar masses are sampled from a Kroupa (2001) initial mass function (IMF) in the range 0.08–150 $M_\odot$. We set the virial radius of the cluster to 1 pc.

As we are focused specifically on massive BHs, we require that at least one BH with a mass greater than 50 $M_\odot$ be present after the first 100 Myr of each model; if no such objects form in a given model or if they are all quickly ejected, we stop the model prematurely. Additionally, we note that one of our models, 1e, produced a massive BH ($M \sim 460\,M_\odot$), which caused a small time step and thus became prohibitively computationally expensive. We argue that this IMBH will most likely not remain in the cluster as BHs of similar masses in other models are ejected.

For the purpose of this paper and for consistency with previous studies, we define the "pair-instability gap" (or "upper mass gap") as BHs with masses in the range 40.5–120 $M_\odot$, as determined by our assumed prescriptions for pair-instability physics (for details, see Belczynski et al. 2016; Kremer et al. 2020a). Furthermore, we use the term "IMBH" to refer specifically to BHs with $M > 120\,M_\odot$, beyond our assumed upper boundary for the pair-instability gap and "massive BH" as a general term to refer to any BH with mass greater than 40.5 $M_\odot$.

In our models we assume that BHs formed from stellar collapse have zero effective spin. This assumption is consistent with predictions of near-zero BH natal spins from theoretical models of angular momentum transport in massive stars (Fuller & Ma 2019; Fuller et al. 2019). We discuss the caveats of this assumption in Section 7.3. Additionally, BHs formed from BH mergers are assigned spins from a distribution that is isotropically distributed on a sphere.

2.1. Binary Fraction

Studies of the Galactic field demonstrate that the binary fractions of O- and B- type stars are nearly 100% (e.g., Sana et al. 2012; Moe & Di Stefano 2017). Furthermore, YMCs, the likely progenitors of GCs, have binary fractions comparable to those seen in the field (e.g., Sana et al. 2009). Thus, it is

Table 1
List of Cluster Models

Model	$f_{b,high}$	$t_{BH,ejec}$ (Gyr)	N_{BH} ($N > 2$gen)	$N_{PI\ gap}$ ($N > 2$gen)	N_{IMBH} ($N > 2$gen)	$M_{BH,max}$ (stellar ev ($M_\odot$))	$M_{BH,max}$ (BH merger ($M_\odot$))	BBH Mergers N_{total}	BBH Mergers $N_{PI\ gap}$	BBH Mergers N_{IMBH}
1a	0.50	3.2	2560 (52)	40 (38)	2 (1)	137	132	143	41	1
1b	0.50	1.3	2543 (46)	29 (27)	0 (0)	90	82	144	43	0
1c	0.50	1.0	2570 (31)	14 (13)	1 (0)	182	211	140	45	1
1d	0.50	1.5	3002 (55)	25 (23)	1 (0)	301	106	163	36	1
1e	0.50	1.2	3120 (22)	5 (3)	1 (0)	430	459	44	6	1
1f	0.50	1.3	2549 (44)	30 (25)	0 (0)	104	77	149	37	0
1g	0.50	1.5	2567 (33)	21 (17)	0 (0)	93	117	130	46	0
1h	0.50	1.2	2548 (43)	22 (21)	1 (0)	125	93	140	36	1
1i	0.50	3.3	2549 (56)	31 (26)	1 (0)	136	155	154	43	1
1j	0.50	2.2	2585 (48)	23 (20)	0 (0)	71	105	146	43	0
1k	0.50	2.1	2562 (41)	32 (26)	1 (0)	146	163	130	40	1
1l	0.50	1.5	2553 (39)	25 (20)	0 (0)	105	114	138	38	0
1m	0.50	1.2	3163 (46)	33 (26)	2 (0)	367	139	130	36	2
1n	0.50	0.5	2545 (30)	23 (20)	0 (0)	91	79	107	37	0
1o	0.50	0.3	2545 (27)	22 (15)	2 (2)	104	153	104	34	0
2a	0.75	2.2	2636 (69)	42 (39)	2 (2)	96	124	204	44	0
2b	0.75	1.1	2663 (51)	32 (26)	1 (0)	170	252	188	51	1
2c	0.75	2.2	2709 (60)	39 (35)	1 (0)	194	257	186	50	1
2d	0.75	2.0	2656 (64)	38 (32)	0 (0)	72	111	186	52	0
2e	0.75	1.1	2648 (50)	30 (27)	1 (0)	146	175	176	40	1
2f	0.75	1.2	2669 (45)	26 (21)	1 (1)	109	120	169	44	0
2g	0.75	2.2	2671 (60)	34 (29)	2 (0)	185	91	186	49	1
2h	0.75	1.3	2620 (53)	44 (41)	0 (0)	83	99	160	47	0
2i	0.75	1.1	2622 (46)	35 (29)	0 (0)	93	117	176	54	0
2j	0.75	1.7	2672 (46)	31 (27)	0 (0)	85	100	172	54	0
2k	0.75	1.5	2626 (45)	27 (26)	0 (0)	85	77	169	41	0
2l	0.75	1.8	2639 (57)	37 (34)	0 (0)	76	86	182	39	0
2m	0.75	0.7	3206 (47)	25 (21)	2 (1)	288	325	137	35	3
2n	0.75	1.2	2628 (49)	39 (31)	0 (0)	97	116	165	49	0
2o	0.75	0.6	2627 (35)	23 (20)	0 (0)	65	118	141	42	0
2p	0.75	0.7	2631 (41)	34 (28)	0 (0)	94	110	141	43	0
2q	0.75	0.2	2612 (31)	29 (21)	0 (0)	89	85	113	29	0
2r	0.75	0.7	2613 (35)	21 (18)	0 (0)	72	107	145	36	0
2s	0.75	1.7	2634 (70)	42 (38)	0 (0)	101	99	197	49	0
2t	0.75	0.7	2724 (40)	25 (20)	1 (0)	193	222	156	46	1
2u	0.75	0.5	2634 (40)	33 (24)	1 (1)	113	142	140	51	0
2v	0.75	0.6	2659 (38)	30 (22)	3 (2)	126	151	144	43	1
2w	0.75	0.6	2678 (37)	28 (24)	2 (0)	197	230	140	47	2
2x	0.75	0.6	2685 (36)	20 (17)	1 (0)	199	222	134	37	1
2y	0.75	0.6	2629 (39)	31 (25)	0 (0)	94	77	147	33	0
3a	1.0	0.1	2711 (31)	25 (21)	1 (0)	168	187	116	26	1
3b	1.0	0.2	2703 (26)	23 (15)	0 (0)	98	69	115	28	0
3c	1.0	2.6	2709 (51)	28 (21)	0 (0)	75	107	190	45	0
3d	1.0	1.7	3249 (70)	36 (25)	2 (0)	280	342	222	48	3
3e	1.0	3.6	2737 (62)	33 (32)	0 (0)	64	111	230	47	0
3f	1.0	0.6	3322 (57)	33 (25)	3 (1)	306	334	190	43	3
3g	1.0	1.7	3109 (76)	42 (38)	3 (0)	261	98	210	52	1
3h	1.0	2.1	3654 (79)	37 (29)	2 (0)	315	348	237	47	2
3i	1.0	2.1	2739 (60)	44 (39)	0 (0)	94	120	209	54	0
3j	1.0	0.6	2725 (56)	36 (31)	0 (0)	94	111	179	39	0
3k	1.0	0.3	2734 (38)	29 (20)	1 (0)	181	67	184	45	1
3l	1.0	0.6	2685 (43)	44 (33)	0 (0)	106	108	174	54	0
3m	1.0	1.7	2749 (78)	39 (33)	2 (2)	103	154	231	48	0
3n	1.0	0.6	3257 (49)	26 (19)	2 (0)	285	118	174	40	1
3o	1.0	1.9	3986 (78)	45 (36)	3 (2)	474	511	208	43	1

Note. List of all cluster models included in this study. In column 2 we indicate the model's primordial high-mass binary fraction. Column 3 lists the time at which the last BH with mass greater than 50 $M_\odot$ escapes the cluster. Column 4 indicates the total number of BHs formed through both stellar collapse or BH merger, with the number of those formed through BH mergers in parentheses. Columns 5–6 indicate the number of BHs formed with masses in the pair-instability gap (40.5–120 $M_\odot$) and number of IMBHs, respectively. Similarly, the number of BHs in these mass ranges formed through BH mergers is noted in parentheses. Columns 7–8 list the masses of the most massive BH formed through stellar collapse and BH mergers, respectively. Columns 9–11 list the total number of binary BH mergers between two stellar-mass BH components, mergers with at least one component in the pair-instability mass gap, and mergers with at least one IMBH, respectively.

possible that even though GCs currently have low binary fractions ($\lesssim$10%), their primordial binary fractions may have been higher in the past (e.g., Ivanova et al. 2005; Milone et al. 2012).

The importance of binaries in star cluster evolution is well known (Heggie & Hut 2003; Chatterjee et al. 2010, 2013). In particular, they act as a dynamical energy source that effectively heats the cluster and slows gravothermal contraction (e.g., Heggie & Hut 2003). In addition, binaries increase stellar collision rates (e.g., Fregeau & Rasio 2007; Bacon et al. 1996) and BH merger rates (e.g., Chatterjee et al. 2017). González et al. (2021) demonstrated that increasing the primordial binary fraction for massive stars from 0 to 1, as suggested by observations (Sana et al. 2012), doubled the number of massive-star collisions and produced BHs with masses within and above the upper mass gap. In this follow-up work, we examine in more detail the influence of binary fractions on BH formation, and study the long-term dynamical evolution and retention of the IMBHs formed in the models.

We define the high-mass binary fraction, $f_{\rm b,high}$, as the fraction of objects with masses above 15 $M_\odot$ that have a companion at the time of cluster formation. For all models, the low-mass (<15 $M_\odot$) binary fraction is fixed at 0.05. This value is motivated by observations of low binary fractions in GCs (e.g., Milone et al. 2012) and detailed studies of the evolution of the binary fraction in dense star clusters (e.g., Fregeau et al. 2009). The $f_{\rm b,high}$ is set to 0.5, 0.75, and 1. We run 15 realizations each for the models with $f_{\rm b,high} = (0.5,\ 1)$ and 25 realizations for those with $f_{\rm b,high} = 0.75$.

For low-mass binaries, primary masses are drawn randomly from the Kroupa IMF, secondary masses are drawn assuming a flat mass ratio distribution in the range 0.1–1 $M_\odot$ (e.g., Duquennoy & Mayor 1991), and initial orbital periods are drawn from a log-uniform distribution $dn/d\log P \propto P$. For the secondaries of the massive stars (>15 $M_\odot$), a flat mass ratio distribution in the range [0.6,1] is assumed and initial orbital periods are drawn from the distribution $dn/d\log P \propto P^{-0.55}$ (e.g., Sana et al. 2012). For all binaries, the initial orbital periods are drawn from the Roche limit (using the stars' ZAMS masses and radii) to the hard–soft boundary, and eccentricities are assumed to be thermal (Heggie 1975).

3. IMBH Formation

Of the total 49 IMBHs formed in 55 simulations, 34 form via the collapse of a massive star grown through repeated stellar collisions and 15 result from BBH mergers of lower-mass BHs (typically involving two or fewer consecutive BBH mergers). The most massive IMBHs form through the collapse of massive stars, as the low escape velocity of GCs makes it difficult to retain BH merger products (as discussed in more depth in Section 5). Figure 1 shows the formation history of an exemplary IMBH from our models. Initially, during a binary–single interaction, all of the masses merge and form a massive remnant (Gurkan et al. 2006). The collision product rejuvenates accordingly and evolves into a giant star that participates in another single–single (SS) collision with a main-sequence star. This is followed by a merger with the component of a binary and ~10 collisions with low-mass main-sequence stars. The final product, a giant with a total mass of roughly 205 $M_\odot$ and core mass of ≈43.7 $M_\odot$, collapses into a BH of ≈185 $M_\odot$.

In Figure 2 we show the normalized mass spectrum of all BHs formed in our models. We distinguish between BHs

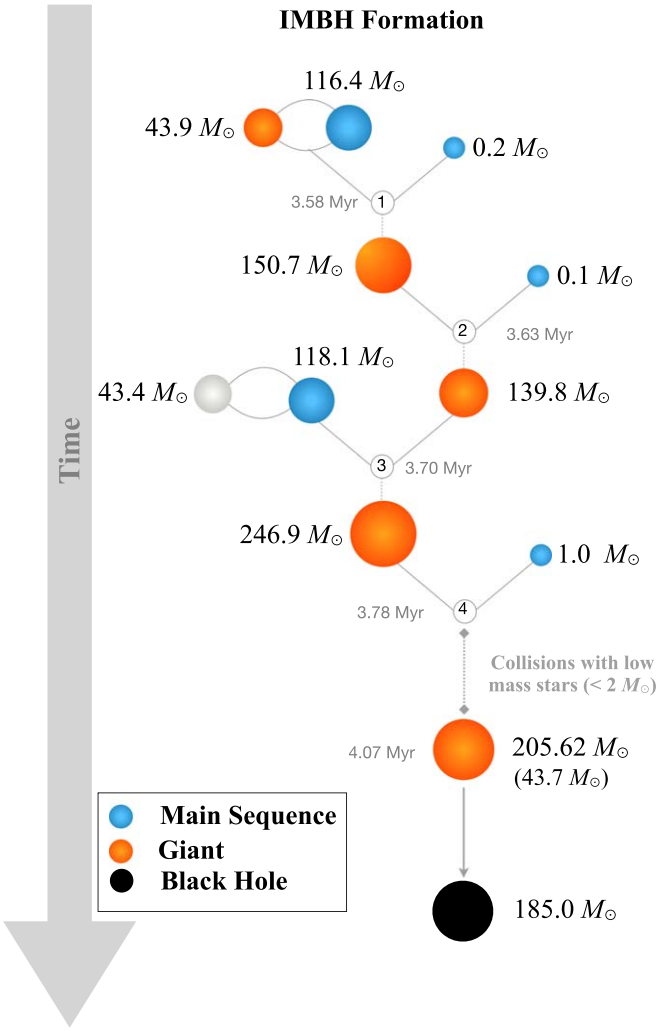

Figure 1. Formation history for one of the IMBHs formed in our cluster models. The color indicates the stellar type and binaries are marked with a loop. The times of each collision are indicated, as well as the masses at the time of the next collision. Lastly, the core mass of the progenitor is indicated in parenthesis. Circles in gray indicate stars that are present in the dynamical interaction but do not contribute to the merger product.

formed via stellar collapse (solid curves) and those produced via BH mergers (dashed curves). As $f_{\rm b,high}$ increases, the masses of BHs formed through stellar collapse skew slightly higher, though this effect is more notable when comparing to the models with zero primordial binaries studied by González et al. (2021), reproduced here as the gray-shaded distribution. At the $f_{\rm b,high}$ examined here, however, the difference is only slight. This trend reflects how binaries increase collision rates in clusters; the extra collisions induced by a higher binary fraction produce a few more stars massive enough to collapse into BHs. As BH mergers are even rarer than stellar collisions, the merger product mass is less noticeably affected by $f_{\rm b,high}$. Even so, Table 1 demonstrates that the $f_{\rm b,high} = 1$ model does in fact produce the highest number of IMBHs. On average, the models with $f_{\rm b,high} = 0.5$ produce ≈0.8 IMBHs per simulation, while in the case of $f_{\rm b,high} = 1$, this number increases to ≈1.3.

We find no clear relation between the formation of an IMBH and the effects it may have on the mass-gap population of BHs. In forming a very massive IMBH, some models exhibit a smaller number of mass-gap BHs, but this is not true in all cases. This reveals that IMBH formation is a random process

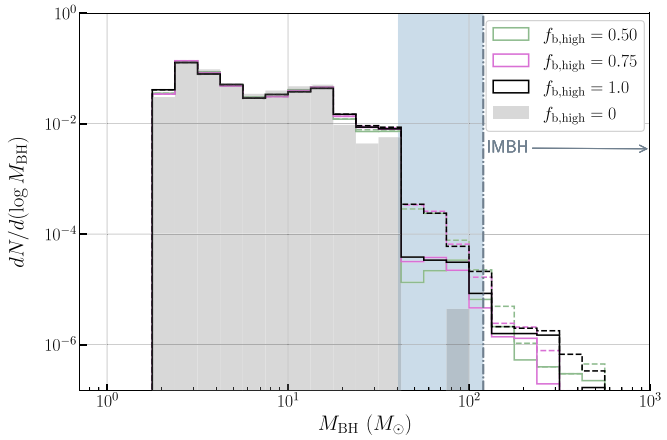

Figure 2. The normalized BH mass spectrum for our models listed in Table 1. The solid lines presented BHs formed through the collapse of a massive star while the dashed lines are products of binary BH mergers. The colors indicate the value for the high-mass binary fraction. The blue shaded region indicates the upper mass gap and the dashed/dotted line the beginning of the IMBH region. The shaded histogram is taken from González et al. (2021).

that affects cluster evolution in ways dependent on the IMBH's specific formation pathway (for example, the number of massive star collisions that were needed to form the IMBH progenitor). This of course, is not the case for the formation of IMBHs with masses $M > 500\,M_\odot$, as this stellar runaway process would leave a stronger impact on the stellar-mass BH population.

4. Companions

In this section we take a closer look at the companions of IMBHs in our models. To do this, we show the time evolution of IMBH binaries in several representative cases in Figure 3. These include a typical IMBH quickly ejected from the cluster (magenta), an IMBH–IMBH binary (blue), and the IMBH that remains in the cluster for the longest period of time (∼500 Myr) across all models (yellow). The dynamical history is shown in three panels, the first showing the companion masses, the second the semimajor axis of the binary, and the third a measure of the eccentricity.

In the first case, the IMBH never stays for long with a consistent binary companion and is quickly ejected from the cluster (at $t \sim 65$ Myr) by a scattering interaction. Repeated exchange interactions during binary–binary and binary–single encounters cause the IMBH to appear in harder, more eccentric binaries until it finally escapes from the cluster with its companion. This particular escaping binary, due to its high eccentricity, has a short inspiral time and will merge within a Hubble time, making it a potentially detectable GW source. This case is typical of most of the IMBHs generated in our models.

The second case that we consider is an IMBH that forms a binary with another IMBH. The primary IMBH initially inhabits multiple wide binaries, with semimajor axes of thousands of au. It eventually settles into a wide binary with another IMBH of $183\,M_\odot$, which steadily hardens through hundreds of interactions before finally gaining enough energy to escape the cluster. Once again, this ejected binary merges within a Hubble time.

Lastly, we examine a case where an IMBH survives in-cluster for a longer period of time. This IMBH is very dynamically active, constantly involved in gravitational scattering interactions. Although it inhabits binaries with other BHs most of the time, it has a main-sequence companion of

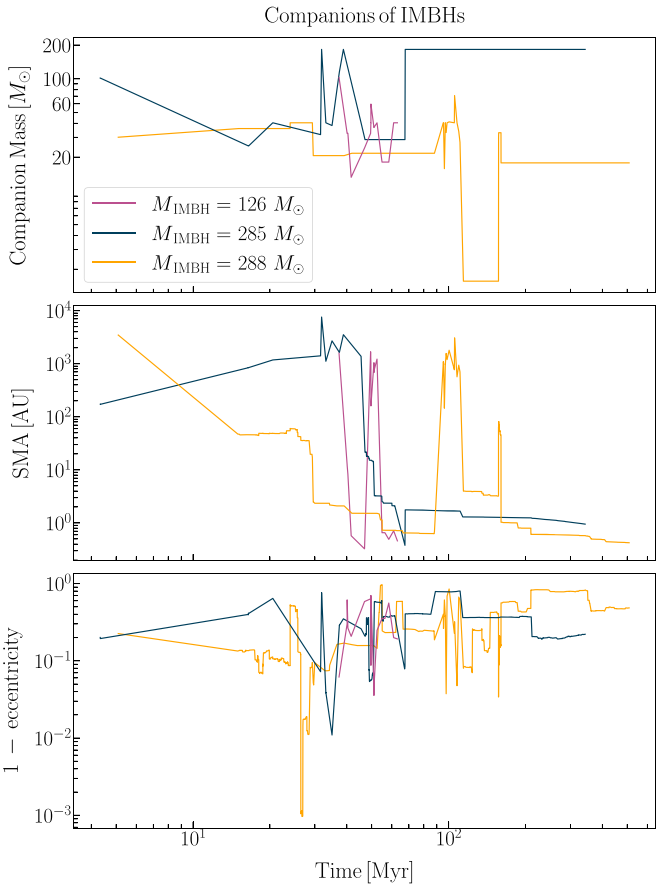

Figure 3. The top panel shows the BH companion masses over time for three separate IMBHs. The middle panel shows the semimajor axes of the different binaries that the IMBH inhabits, and the bottom panel plots the eccentricity.

roughly $1.6\,M_\odot$ during the later stages, before it exchanges into a binary with another BH, with which it merges during a binary–binary encounter. The GW recoil kick imparted on the IMBH causes it to escape the cluster in a binary that will merge within a Hubble time.

Approximately 65% of the IMBHs in our models are ejected within the first 100 Myr. The reason for these ejections is explored in Section 5. The characteristic examples above all feature numerous close scattering interactions, demonstrating that IMBHs formed in clusters are very dynamically active. The most common companions to the IMBHs are other BHs, with only a few instances of main-sequence companions.

Binaries between a star and an IMBH are of interest due to their possible detection using radial velocity measurements of star clusters (Giesers et al. 2019; Kamann et al. 2021). However, in our models, we only observe one star–IMBH binary with a low-mass main-sequence star ($M < 2\,M_\odot$) that is constantly perturbed by other objects in the cluster (every ∼0.003 Myr, on average). Thus, indirect measurements of IMBHs with masses like those explored in this paper using this method seems unlikely.

An additional observational signature is the tidal disruption of a star by an IMBH, which could produce strong electromagnetic signatures (Ramirez-Ruiz & Rosswog 2009; Chen & Shen 2018; Kremer et al. 2022). We count approximately 20 candidates (95% of which are on the main sequence) for such events in our simulations (i.e., instances where a star passes within the classical disruption radius of an IMBH; see Kremer et al. 2022). F. Kıroğlu et al. (2022, in preparation) investigates tidal

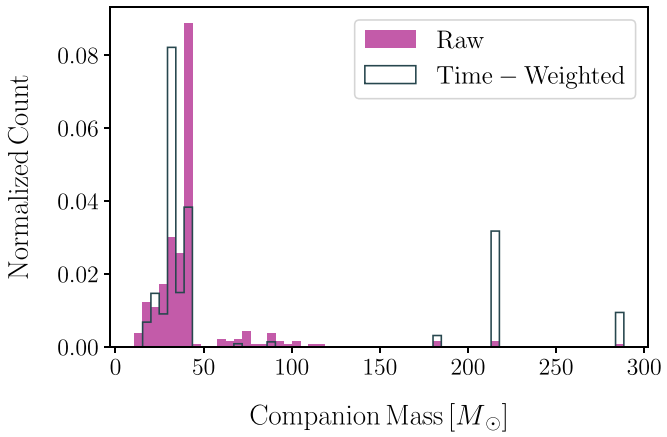

Figure 4. In magenta we show the raw distribution of the masses of the BH companions of IMBHs. The blue outline is the companion mass distribution weighted by the lifetime of the binary.

disruptions involving stars and IMBHs of similar masses using the smoothed-particle hydrodynamical simulation `StarSmasher`.

To study the BHs that accompany the IMBHs, we plot the distribution of their masses as the filled magenta histogram in Figure 4. The blue outline shows the same distribution, weighted by the amount of time that each of these companions spends in the binary with the IMBH. As can be inferred from the plot, the most common companions are BHs with masses roughly in the range 30–40 $M_\odot$. This is because BHs in this mass range are massive enough to survive dynamical interactions with other BHs (i.e., not be replaced in the binary during exchange interactions).

5. IMBH Ejection

IMBH ejection from star clusters primarily occurs through two distinct mechanisms: recoil kicks from BH mergers and dynamical kicks from strong binary-mediated gravitational scattering encounters. In the first case, which dominates, anisotropic emission of GWs during a BH merger gives the merger remnant a recoil kick determined by the mass ratio of the system and the initial spins of the BHs (Merritt et al. 2004; Campanelli et al. 2007; Lousto & Zlochower 2008). In general, near-equal-mass binaries and low-spinning (as well as aligned) BHs will receive smaller kicks and thus are most likely to be retained in the cluster. Our assumption that BHs are born with zero spin increases the retention likelihood for first-generation mergers. However, as the merger remnant typically receives a significant spin, any later mergers are more likely to eject the product from the cluster, lowering the rate of 2G+ mergers in GCs (see, e.g., Rodriguez et al. 2019, for an overview of repeated BH mergers in dense star clusters). Overall, GW recoil kicks account for 64% of the IMBH ejections in our models.[6]

[6] Of course, these fractions are specific to the cluster mass adopted in our simulations and will change for clusters with different masses and hence different escape velocities. For example, see Mahapatra et al. (2021) for a study of BH retention in both nuclear and globular star clusters. Of the IMBH ejections in our models, 84% occur during 1G + 1G mergers (first-generation), 10% during 1G + 2G mergers, and 6% during 2G + 2G mergers. The low mass ratios—and correspondingly strong GW recoil kicks—typical of mergers between IMBHs and smaller companions are partially responsible for the high fraction of ejections during first-generation mergers. These mergers, which can occur in isolated binaries or during binary–single or binary–binary interactions, are also promising GW sources, which we discuss in Section 6.

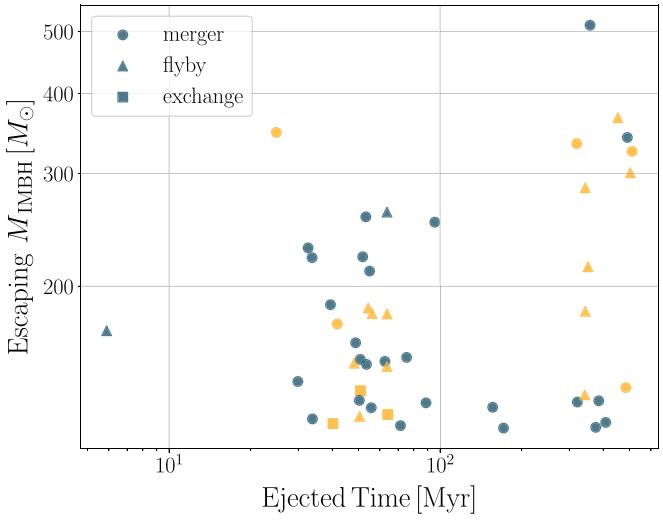

Figure 5. Mass of IMBHs as a function of the ejection time from the cluster. The IMBHs escaping in a binary are indicated in yellow, while those escaping as single objects are marked in blue. The different shapes indicate the dynamical interactions responsible for the ejection of the IMBHs.

Strong gravitational scattering encounters can also eject IMBHs from clusters. Recall that scattering interactions in star clusters typically harden binaries (Heggie 1975), where passing objects (singles or binaries) on average gain kinetic energy as the binary components sink deeper into their mutual potential well. This can be conceptualized as an exchange between the binary binding energy and the orbital energy of the passing objects in the global cluster potential. Conservation of momentum, however, guarantees that any velocity change experienced by the passing object is countered by a change to the velocity of the binary's center of mass. So potential energy from the binary components not only gives a recoil velocity to the passing object, but also to the binary itself. These recoil kicks can be large enough to eject an IMBH involved in such an encounter.

Figure 5 plots the masses of ejected IMBHs in our models as a function of the time of escape from the cluster. Circles indicate IMBHs ejected by GW recoil kicks received during BH mergers while triangles indicate flyby interactions, where the initial configuration of objects remains unchanged. In this case, if the IMBH is the passing object, it will extract energy from a binary during the flyby and as a result gain a velocity kick, sometimes larger than the escape speed of the cluster. This, in turn, hardens the binary (usually a BH binary), sometimes to the point of merger. A similar output can be expected if the IMBH is originally a member of the binary instead and experiences a flyby with a single BH. Lastly, the squares represent exchange interactions during which the IMBH is exchanged into a binary (yellow) or out of its original binary (blue). This case is favored when the intruder's mass exceeds that of either binary component. Furthermore, the new binary resulting from the exchange has a higher binding energy as a result. Whether the final single star or binary receive kick velocities large enough to eject them from the cluster depends on the initial velocity of the single star as well as the semimajor axis of the binary. It is clear from Figure 5 that the merger channel is the most efficient at ejecting massive BHs from clusters.

In Figure 6 we show the properties of the systems responsible for IMBH ejection during binary–single and

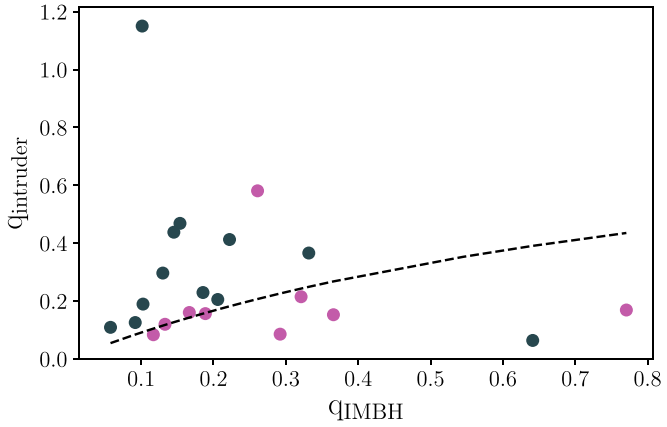

Figure 6. Mass ratios of an interaction involving an IMBH–BH binary and an intruder. The horizontal axis shows the mass ratio between the IMBH companion and the IMBH while the vertical axis shows the mass ratio with the intruder. The color indicates if the intruder is a single object (magenta) or a binary (blue). The dashed line indicates an intruder with the same mass as the IMBH companion for cases where the intruder is a single object.

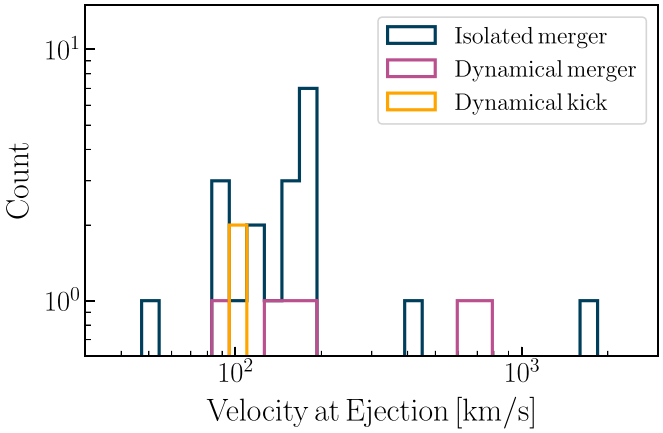

Figure 7. Escape velocities [initial speed+kick velocity] of single IMBHs ejected from the clusters in km s^{-1}. The subpopulations indicate IMBHs ejected due to strong GW recoil kicks during isolated BH mergers (blue) and dynamical mergers (magenta), as well as IMBHs receiving velocity kicks during strong dynamical interactions (yellow).

binary–binary interactions if the IMBH was originally in a binary, which is often the case. Along the horizontal axis we plot the mass ratio for the binary containing the IMBH, defined as $q_{\rm IMBH} = \frac{m_{\rm comp}}{m_{\rm IMBH}}$. In the case of binary–single interactions (shown in magenta), the vertical axis, $q_{\rm intruder}$, is the mass ratio of the single intruder to total mass of the binary ($q_{\rm intruder} = \frac{m_{\rm intruder}}{m_{\rm comp}+m_{\rm IMBH}}$). For binary–binary interactions (shown in blue), $q_{\rm intruder}$ is the ratio between the total mass of the intruder binary and the IMBH–BH binary. The dashed line indicates the case where the intruder mass is equal to the mass of the IMBH companion ($m_{\rm intruder} = m_{\rm comp}$).

This plot shows that, in general, $m_{\rm intruder} \gtrsim m_{\rm comp}$ is necessary to eject the IMBH—though this is not always the case, as some binaries have already been influenced dynamically by previous interactions.

5.1. Singly Ejected IMBHs

Out of the 48 escaping IMBHs, 28 escape the cluster as single BHs. Table 2 lists the distribution of ejection methods for singly ejected IMBHs in each model. The second column indicates the number of singly ejected IMBHs per model. The third column records the number of BHs ejected due to GW recoil kicks received during a merger. These mergers can occur in isolated binaries or during strong dynamical interactions, and this difference is taken into account in the table. It is important to note that dynamical hardening during earlier scattering interactions may have significantly hastened mergers labeled as isolated. Lastly, the rightmost column counts IMBHs ejected due to velocity kicks received during dynamical interactions (shown as flybys or exchanges in Figure 5).

To further study the properties of these ejected IMBHs, Figure 7 shows the distribution of velocity kicks that singly escaping IMBHs received for each of the ejection scenarios. The highest IMBH ejection velocities result from BH mergers (blue and magenta). The bimodality of the GW recoil velocity distribution is attributable to 2G + mergers, which have higher recoil kicks. The scarcity of high ejection velocities reflects the early ejection of most IMBHs, which are then unable to participate in 2G + mergers. As the extreme mass ratio typical of an IMBH encounter with smaller objects damps any dynamical kick, BHs ejected due to dynamical interactions experience lower ejection velocities (though still well above the typical GC escape speed of ∼60 km s^{-1}).

Table 2
Singly Ejected IMBHs

$f_{\rm b,high}$	$N_{\rm bh}$ (single)	$N_{\rm GW\ recoil}$ (iso. bin.)	$N_{\rm GW\ recoil}$ (dyn.)	$N_{\rm dyn}$
0.50	6	5	1	0
0.75	13	9	3	1
1.0	9	6	2	1

Note. For each set of models with distinct $f_{\rm b,high}$ (column 1), column 2 lists the total number of singly escaping IMBHs from that model set. Columns 3–4 list the number of IMBHs ejected due to the large GW recoil kicks received during an isolated binary merger or dynamically induced merger, respectively. Column 5 lists the number of IMBHs ejected by large velocity kicks from dynamical interactions.

5.2. IMBHs Escaping in Binaries

The remaining 20 IMBHs escape in binaries, and depending on their inspiral times, can be interesting sources of GWs. To study the IMBHs that are ejected in binaries, we plot the binary mass ratio (q) as a function of the escaping IMBH mass in Figure 8. We see that the majority of the IMBHs ejected in binaries have inspiral times that would make them potential GW sources detectable by current and future detectors such as LIGO/Virgo/Kagra and LISA. Furthermore, four IMBHs escape the cluster in a binary with another massive BH (as shown by the four points above the blue dashed line), while most are ejected with stellar-mass BHs.

The short inspiral times can be attributed to binary hardening through dynamical interactions in the cluster. An example of this is shown in Figure 9, which illustrates the dynamical history of a case in which the binary merges within a short inspiral time after ejection from the cluster. Initially, the IMBH is a single object that forms a binary with a 31 $M_\odot$ BH. After ≈280 Myr, during an interaction with another BH binary, the IMBH exchanges into a new binary with a smaller separation before experiencing a velocity kick large enough to eject it from the cluster. This binary eventually merges in ≈3 Gyr.

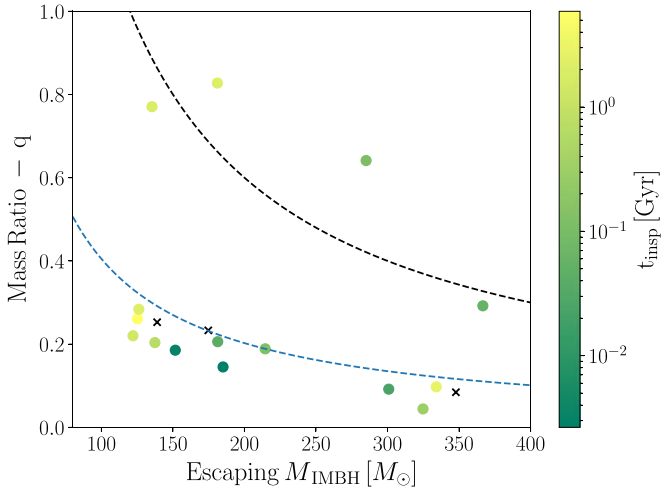

Figure 8. Mass ratio as a function of the IMBH mass in escaping binaries. The color gradient indicates the inspiral times. The crosses label binaries that do not merge within a Hubble time ($t_{\rm inspiral} \geqslant 12$ Gyr). The inspiral times are calculated using the Peters equation (Peters 1964), taking the eccentricity and separation of the binary into account. The dashed blue and black curves indicate companions with masses larger than 40 and 120 $M_\odot$, respectively.

6. BBH Mergers

The total number of BBH mergers is listed in column 9 of Table 1. Columns 10 and 11 list the number of mergers where at least one component is in the upper mass gap or an IMBH, respectively. Note that the ratio of mass-gap mergers to stellar mergers is higher than estimates in previous CMC studies (e.g., Rodriguez et al. 2019; Kremer et al. 2020a) and GW observations (e.g., Abbott et al. 2020) simply because the models were interrupted at early times. Thus, we do not account for stellar-mass BH mergers that occur at later evolutionary stages of these clusters.

As we have discussed in previous sections, IMBHs in our models tend to form binaries with other BHs deep in the core of their host cluster. This leads, in some occasions, to in-cluster IMBH–BH mergers. Additionally, ≈42% of the IMBHs are ejected in binaries with other BHs, most of which will merge within a Hubble time. Some of these mergers may be detectable today as GW sources in either high- or low-frequency bands. We now examine these mergers in detail before discussing merger rate implications for modern GW detectors.

6.1. IMBH–BH Mergers

Table 3 lists the BBH mergers involving IMBHs. When the merger occurs in the cluster, the merger remnant usually escapes the cluster after receiving a sufficiently high GW recoil kick. There are three instances where the IMBH is retained after a BBH merger, the first in model 1e, which, as mentioned in Section 2, is the model left unevolved due to computational cost. The second instance is in model 3d, where the IMBH merges with its 27 $M_\odot$ BH companion during a binary–binary encounter with another BH binary (with masses 40.5 $M_\odot$ and 30.9 $M_\odot$). Rather than being ejected, the IMBH remains in a binary with the 30.9 $M_\odot$ BH, until ejection during a merger in a binary–single interaction ∼170 Myr later (listed in the table as well). A similar process occurs in model 2 m.

Out of 34 total BBH mergers involving an IMBH, 25 are with stellar-mass BHs and 7 with upper-mass-gap BHs. The remaining two are IMBH–IMBH mergers. The likelihood of these massive remnants to be ejected from the cluster prevents any further later-generation mergers.

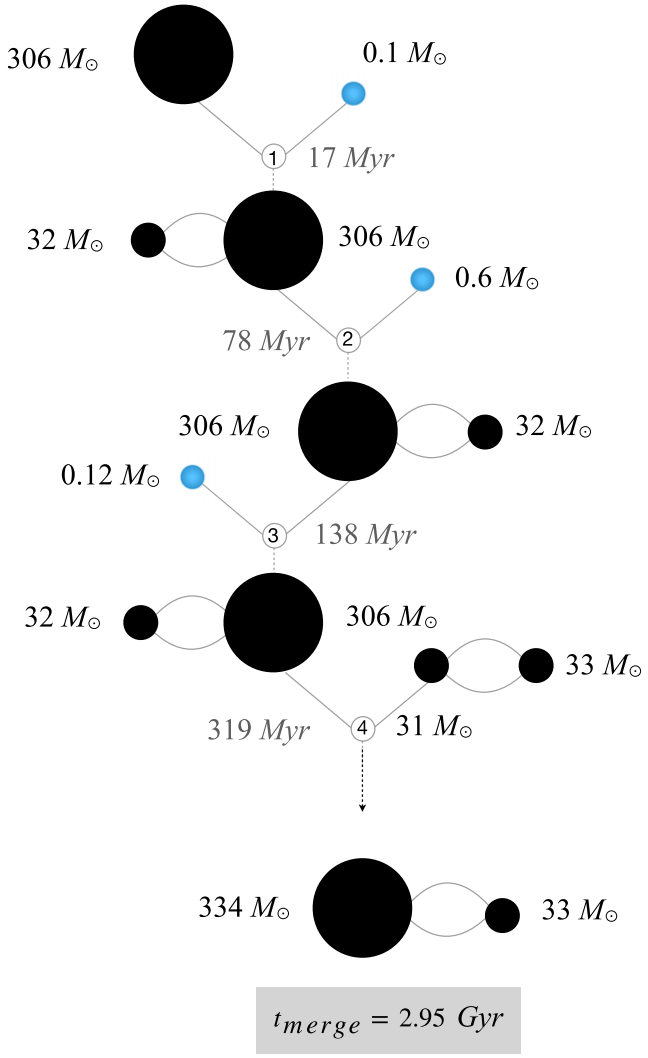

Figure 9. Example of an escaping BH binary that merges within a Hubble time.

The distribution of eccentricities at a GW frequency of 10 Hz for all in-cluster IMBH–BH mergers has a median value of 10^{-4}, decreasing to 10^{-7} for ejected binaries. These results are consistent with a study of BBH mergers in dense star clusters by Rodriguez & Loeb (2018). However, we find that 12% of IMBH–BH mergers enter the LIGO frequency band with detectable eccentricities ($e > 0.05$). These high-eccentricity mergers occur specifically when two BHs merge during a binary-mediated interaction.

The distribution of spins in our IMBH–BH mergers generally peaks at two different values. Most of the BHs have close to zero spin (as expected, based on our BH natal spin assumption), and the other population shows spins at about 0.7. See Rodriguez et al. (2019) for a full study of the fate of BHs resulting from repeated mergers in dense star clusters with different assumptions of BH natal spins.

6.2. Merger Rates

We now estimate merger rates for BH binaries that merge inside the cluster as isolated binaries or through dynamical interactions, as well as ejected binaries with inspiral times less

Table 3
Mergers Involving an IMBH

Model	$t_{\rm merge}$ (Gyr)	M_1 ($M_\odot$)	M_2 ($M_\odot$)	Type	Outcome	$t_{\rm eject}$ (Gyr)
1a	0.77	28.0	137.4	Ejected Binary	N/A	0.05
1 c	0.05	32.7	182.1	isolat-binary	Ejected	N/A
1d	0.53	27.6	300.9	Ejected Binary	N/A	0.5
1e	1.04	429.7	32.2	isolat-binary	Retained	N/A
1h	5.94	32.7	125.2	Ejected Binary	N/A	0.05
1i	0.08	20.9	136.2	isolat-binary	Ejected	N/A
1k	0.05	19.6	145.6	isolat-binary	Ejected	N/A
1 m	0.48	18.8	122.1	binary–binary	Ejected	N/A
1 m	0.51	366.6	107.1	Ejected Binary	N/A	0.45
2b	0.1	92.7	170.0	isolat-binary	Ejected	N/A
2 c	0.05	194.2	71.0	binary–single	Ejected	N/A
2e	0.04	32.4	146.0	binary–binary	Ejected	N/A
2g	0.06	26.9	185.0	Ejected Binary	N/A	0.05
2 m	0.09	21.7	288.5	isolat-binary	Retained	N/A
2 m	0.51	17.8	308.3	binary–binary	Ejected	N/A
2 m	0.83	14.4	324.8	Ejected Binary	N/A	0.51
2t	0.03	32.6	192.6	isolat-binary	Ejected	N/A
2v	2.32	35.8	126.1	Ejected Binary	N/A	0.06
2w	0.03	36.8	196.8	binary–single	Ejected	N/A
2w	0.05	28.1	151.6	Ejected Binary	N/A	0.05
2x	0.05	25.9	199.1	isolat-binary	Ejected	N/A
3a	0.04	21.3	168.0	isolat-binary	Ejected	N/A
3d	0.32	280.0	27.0	binary–binary	Retained	N/A
3d	0.49	41.3	304.5	binary–single	Ejected	N/A
3d	0.48	40.5	214.5	Ejected Binary	N/A	0.35
3f	0.32	31.3	305.7	binary–binary	Ejected	N/A
3f	3.27	334.1	32.5	Ejected Binary	N/A	0.32
3f	2.38	104.3	135.4	Ejected Binary	N/A	0.34
3g	2.26	181.1	149.8	Ejected Binary	N/A	0.06
3h	0.02	36.8	314.6	binary–single	Ejected	N/A
3h	1.56	122.1	26.9	Ejected Binary	N/A	0.04
3k	0.1	37.3	181.3	Ejected Binary	N/A	0.06
3n	0.46	182.8	285.0	Ejected Binary	N/A	0.34
3o	0.36	474.4	40.5	isolat-binary	Ejected	N/A

Note. List of all of the BBH mergers with an IMBH component, with the model in which the merger occurs indicated in column 1. Column 2 lists the time at which the merger occurs after cluster formation while columns 3–4 show the component masses. Column 5 lists the mechanism that leads to the merger, with "Ejected Binary" indicating escaping binaries that merge after ejection from the cluster. Lastly, columns 6–7 list the merger outcome and time at which the cluster ejects the merger remnant, respectively.

than a Hubble time. To calculate the volumetric BBH merger rates as a function of the redshift, we use a similar approach as in O'Leary et al. (2009) and Rodriguez et al. (2016), where the comoving merger rate is defined as:

$$\mathcal{R}(z) = \frac{dN(z)}{dt} \times \rho_{\rm GC} \times f. \quad (1)$$

Here $\frac{dN(z)}{dt}$ is the number of mergers per unit time per cluster at a given redshift, $\rho_{\rm GC}$ is the volumetric density of GCs in the local universe—for which we assume a constant value of $\rho_{\rm GC} = 2.31\,{\rm Mpc}^{-3}$ (e.g., Rodriguez et al. 2015; Rodriguez & Loeb 2018)—and f is a scaling factor that accounts for the cluster mass function.

We compute $\frac{dN(z)}{dt}$ from the list of merger times $t_{\rm merge}$ for all BBHs in (or ejected from) our models that merge within a Hubble time $t_{\rm Hubble}$. We use $t_{\rm Hubble} = 13.7$ Gyr and randomly sample 100 cluster ages, $t_{\rm age}$, for each merger from the distribution in El-Badry et al. (2018) with the appropriate metallicity ($Z = 0.1\,Z_\odot$). We then define the effective time at which these mergers occur as $t_{\rm eff} = t_{\rm Hubble} - t_{\rm age} + t_{\rm merger}$ (e.g., Kremer et al. 2020a). $\frac{dN(z)}{dt}$ then simply follows by converting $t_{\rm eff}$ from units of time to redshift and computing the number of BBH mergers per redshift bin. Finally, the rate is normalized by the number of cluster ages sampled and the number of models in our study.

Previous studies have shown that the number of BBH mergers increases roughly linearly with the cluster mass (e.g., Rodriguez et al. 2016; Kremer et al. 2020b)—though this relation may not hold well for clusters that form few massive stars or retain few BHs, e.g., clusters born with top-light stellar IMFs (Weatherford et al. 2021). To account for the higher-mass end of the cluster initial mass function, we incorporate an uncertain factor f as a scaling factor in the rate calculation. To estimate this number, we use the method described in Rodriguez et al. (2015), where f is the number of mergers obtained by integrating the linear relation between the number of BBH mergers and total cluster mass over a normalized cluster mass function divided by the average number of BBH mergers per cluster in the models sampled. Kremer et al. (2020b) applied this calculation to a catalog of CMC simulations that cover the full range of GC properties observed in the Milky Way. The range of initial GC properties we use falls within the range covered by the catalog, so we adapt their best-fit curve for the relationship between the number of BBHs and the cluster mass function for $r_v = 1$ pc (Equation (15) in Kremer et al. 2020b), which yields $f = 4.65$. Our use of this scaling factor is justified with the following reasoning. First, the only difference in the set of initial cluster conditions is the high-mass binary fraction, which is kept at 5% in Kremer et al. (2020b). We do not expect the relationship between the total number of BBH mergers and total cluster mass to change for different binary fractions (as both the total cluster mass and number of BHs slightly increase with the binary fraction), so the linear relationship would still hold. Second, the average number of BBH mergers per cluster remains fairly similar ($\sim$150 in our models, while $\sim$100 in theirs). Furthermore, Weatherford et al. (2021) showed that for cluster models with an initial top-heavy IMF, which produce 10 times as many BHs as our models, the relationship between the total cluster mass and number of BBHs remains fairly linear (see Equation (2) in Weatherford et al. 2021).

Subsequently, the cumulative merger rate is calculated as

$$\mathcal{R}_c(z) = \int_0^z \left(\mathcal{R}(z') \times \frac{dV_c}{dz'} \times (1+z')^{-1} \right) dz', \quad (2)$$

where $\mathcal{R}(z')$ is the comoving merger rate as described in Equation (1), $\frac{dV_c}{dz'}$ is the comoving volume at redshift z' and $(1+z')^{-1}$ corrects for time dilation.

We show in Figure 10 the cumulative and volumetric rates for different BH mass bins. We estimate a total BBH merger rate in the local universe ($z < 0.2$, to be consistent with the LVK Collaboration) of about $20\,{\rm Gpc}^{-3}\,{\rm yr}^{-1}$, which is consistent with the latest rate reported by the LIGO Collaboration, 17.9–$44{\rm Gpc}^{-3}\,{\rm yr}^{-1}$ (The LIGO Scientific Collaboration et al. 2021d). Furthermore, in our models, the IMBH merger rate peaks at $z \approx 2$ with a value of about $2\,{\rm Gpc}^{-3}{\rm yr}^{-1}$; the rapid decrease in the IMBH merger rate at

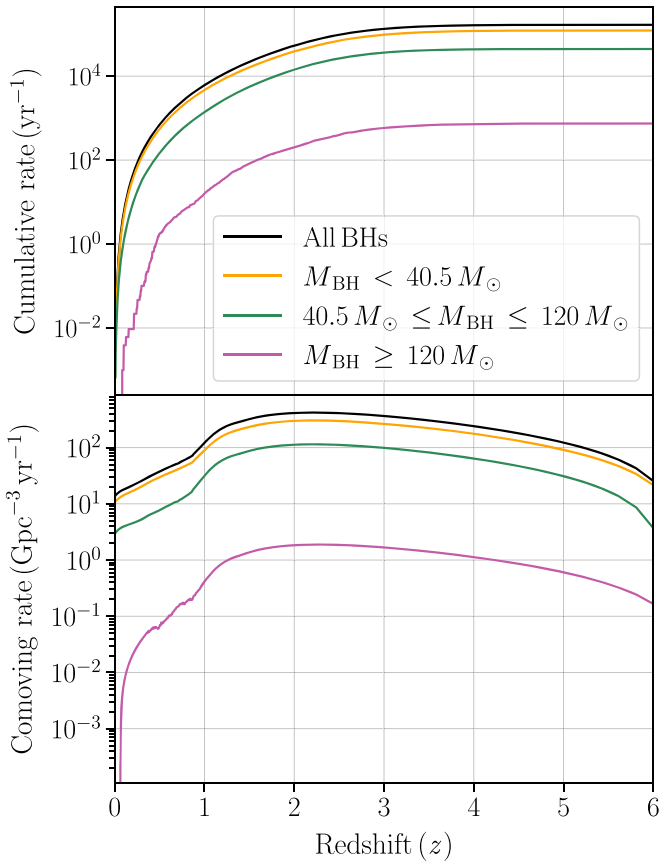

Figure 10. Top panel: cumulative BBH merger rate for BHs, computed using Equation (1). Bottom panel: comoving merger rate calculated with Equation (2). We label as *stellar* mergers cases where both component masses are less than 40.5 $M_\odot$. The green and magenta lines show the merger rates for BBHs with at least one component in the "mass gap" (40.5–120 $M_\odot$) or an IMBH ($M > 120\,M_\odot$), respectively.

lower redshift is due to the dynamical ejection of IMBHs from the cluster. Note that rate calculations in this paper do not include clusters of lower-mass (such as open clusters), which could further increase merger rates (e.g., Di Carlo et al. 2019).

It is not clear whether the scaling factor f used in the method described above remains true for IMBH mergers at the high end of cluster mass. In such clusters, some of these IMBHs could be retained for longer periods of time due to higher escape velocities. Thus, we compute an order-of-magnitude merger rate calculation using the general approach as in González et al. (2021). We define $f_{\rm SF}$ as the fraction of the star formation assumed to occur in star clusters that may produce an IMBH, computed using

$$f_{\rm SF} \approx \frac{\int_{10^4}^{10^6} M^{-2}\,dM}{\int_{10^2}^{10^6} M^{-2}\,dM} \approx 0.01, \quad (3)$$

where we take $10^4\,M_\odot$ as the minimum cluster mass to produce an IMBH. We also assume a minimum value of $10^2\,M_\odot$ for a cluster mass function covering the entire star formation rate (Lada & Lada 2003). Finally, the volumetric rate of IMBH mergers at redshift z is defined as

$$\Gamma(z) \approx \frac{N_{\rm IMBH}}{M_{\rm cl}}\,\rho_{\rm SF}(z)\,f_{\rm SF}, \quad (4)$$

where $N_{\rm IMBH}$ is the average number of IMBHs formed per model, $M_{\rm cl} \approx 5 \times 10^5\,M_\odot$ (the initial cluster mass in our models), and $\rho_{\rm SF}(z)$ is the star formation rate density at redshift z. We determine a value of 0.1 $M_\odot$ Mpc^{-3} yr^{-1} for $\rho_{\rm SF}$ at $z \approx 1$ (e.g., Hopkins & Beacom 2006), when metallicities of 0.1 $Z_\odot$ are relevant. This yields an IMBH merger rate for the models with $f_{\rm b,high} = 1$ (where $N_{\rm IMBH} = 1.27$) of $\Gamma \approx 2.5$ Gpc^{-3} yr^{-1}, a value in agreement with the one calculated above. The IMBH merger rate for the models with $f_{\rm b,high} = 0.75$ and $f_{\rm b,high} = 0.5$ are $\Gamma \approx 1.6$ Gpc^{-3} yr^{-1} and $\Gamma \approx 1.4$ Gpc^{-3} yr^{-1}, respectively.

In a study of the cosmic evolution of BBHs in different star clusters using `FASTCLUSTER` and `CosmoRate`, Mapelli et al. (2022) calculated a local BBH merger rate of 4–8 Gpc^{-3} yr^{-1} in GCs. This is consistent with previous studies on the redshift evolution of the BBH merger rate by Rodriguez & Loeb (2018) and Fragione & Kocsis (2018), which predicted a local rate of 4–18 Gpc^{-3} yr^{-1}. We find that the local ($z \approx 0$) merger rate is 13.9 Gpc^{-3} yr^{-1}, in agreement with Rodriguez & Loeb (2018).

7. Discussion and Conclusions

In this section we review the results of this study and discuss sources of uncertainty that will be the focus of future work.

7.1. Summary

We have studied the primordial high-mass binary fraction's influence on BH formation in dense star clusters. We observe that at high binary fractions, our models exhibit a tail in the BH mass distribution extending to 500 $M_\odot$, beyond the BH upper mass gap and well into the IMBH mass range.

We focus our study on the formation, dynamical evolution, and ejection of IMBHs born with masses in the range 120–500 $M_\odot$. A large fraction (∼70%) are born from the direct collapse of a massive star formed from consecutive stellar collisions between main-sequence stars and evolved giants. We explore the uncertainties in this formation channel in Section 7.3. The remaining IMBHs are products of BH mergers with massive components.

We have also explored the typical companions of IMBHs in the cluster, noticing a preference toward BHs of masses in the range ∼30–40 $M_\odot$. These binaries are usually short-lived as few-body encounters in the dense cluster core frequently exchange new companions into the IMBH binaries. Eventually, the large number of dynamical interactions will either harden the IMBH–BH binaries to the point of merger, or give the binaries large enough velocity kicks to eject them from the cluster.

In a study of the dynamical ejection of IMBHs from GCs using the `MOCCA` code (Giersz et al. 2014)—which uses a Monte Carlo cluster modeling approach similar to `CMC`—Maliszewski et al. (2022) finds that some IMBHs are retained until a Hubble time. However, the effect of GW recoil kicks due to BBH mergers was not taken into account in the simulations, and thus the IMBHs were more likely to be retained. Indeed, we find that all of the IMBHs in our models are ejected from the clusters within the first ∼500 Myr. We explore the mechanisms responsible for these ejections, and discover that most IMBHs are ejected due to the large GW recoil kicks resulting from BH mergers. Some of these IMBHs are ejected in binaries, and we showed that 85% of these binaries merge within a Hubble time and thus are possible

sources of GWs detectable by current (LVK) and second-generation (LISA) interferometers.

Lastly, in Section 6.2 we estimate a BBH merger rate of $19.8\,\mathrm{Gpc^{-3}\,yr^{-1}}$ at $z = 0.2$. This is within the range predicted in previous studies of BBH mergers in star clusters (e.g., Rodriguez & Loeb 2018). We also calculate a maximum IMBH merger rate of $\approx 2\ \mathrm{Gpc^{-3}\,yr^{-1}}$ at $z \approx 2$.

7.2. Ejected IMBHs as Seeds of SMBHs

Observations of quasars (QSOs) at high redshifts ($z \gtrsim 6$) indicate the presence of supermassive BHs (SMBHs) in the first billion years of the universe (e.g., Fan et al. 2006; Decarli et al. 2018). The formation and rapid growth of these objects challenge current theoretical models and have sparked debate on possible formation scenarios (for the most recent review, see Inayoshi et al. 2020). Current formation channels include the collapse of a massive Population III star that forms stellar-mass BH seeds (e.g., Stacy et al. 2012; Hirano & Bromm 2017; Kimura et al. 2021), "heavy-seed scenario" where the collapse of a massive gas cloud forms a BH of $M \approx 10^4$–$10^5\,M_\odot$ (e.g., Oh & Haiman 2002; Mayer et al. 2010), and the formation of BH seeds via repeated stellar mergers (e.g., Zwart & McMillan 2002; Tagawa et al. 2020) or runaway stellar-mass BH mergers in dense star clusters (e.g., Davies et al. 2011; Kroupa et al. 2020).

The IMBHs ejected in our models could be promising BH seed candidates for high-redshift SMBHs. This formation channel is explored in Katz et al. (2015), where metal-poor, high-redshift nuclear star clusters (NSCs) are modeled using high-resolution hydrodynamical cosmological zoom-in simulations as well as direct *N*-body simulations. The study finds that high-redshift NSCs are likely hosts of very massive stars (VMSs) that can collapse into IMBHs. These IMBHs can later grow to masses within the range observed powering high-redshift quasars, if they accrete at the Eddington rate. However, recent studies made with high-resolution cosmological simulations and direct *N*-body integration of seed BH trajectories found that isolated IMBHs do not have time to sink to the centers of galaxies (Ma et al. 2021; Pfister et al. 2019). A potential solution would be for the IMBHs to remain embedded in the host cluster, and efficiently transported to the Galactic center. Even though all of the IMBHs in our models are ejected from the cluster, this may change for more massive IMBHs and/or in more massive star clusters. More detailed theoretical modeling of massive star evolution at very low metallicities, as well as new observational constraints (e.g., from JWST) on the masses and demographics of young, massive star clusters in the early universe, will be needed to better assess this formation channel for high-redshift quasars.

7.3. Caveats and Future Work

The most common massive BH formation process in our models is through repeated stellar collisions that form a very massive progenitor. Uncertainties on the properties of the collision products as well as the exact mass boundaries at which pair instability affects the evolution of the star result in corresponding uncertainties for this formation model.

As a first step to address these uncertainties, Ballone et al. (2022) simulate the collision of two massive stars and follow the structure of the remnant with the smoother-particle hydrodynamics (SPH) code `StarSmasher` (Gaburov et al. 2010). The stars involved in this collision are a core helium-burning (CHeB) star, with mass $M_{\mathrm{CHeB}} = 57.6\,M_\odot$ and a main-sequence (MS) star with mass $M_{\mathrm{MS}} = 41.9\,M_\odot$, consistent with a stellar collision in the dynamical simulations of Di Carlo et al. (2020) and with typical collisions seen in our models. The study shows that the stellar remnant only loses 12% of the total initial mass during the merger, allowing it to collapse into a massive BH at a later time.

In a companion paper, Costa et al. (2022) carefully model the evolution of the stellar collision product using `PARSEC` and `MESA`. They find that the remnant successfully avoids the PI gap and collapses into a BH of mass $\approx 87\,M_\odot$. These results need to be generalized to mergers between different masses and metallicities. Nevertheless, it is the first step in the right direction to study the evolution of massive collision products.

In this study, we have only considered clusters of a specific metallicity ($Z = 0.1\,Z_\odot$). However, lower metallicities will decrease the mass loss in massive stars and thus lead to more massive remnants. Indeed, Giacobbo & Mapelli (2018) show that BH masses in merging BHs strongly depend on the progenitor's metallicity. In a study of the impact of metallicity in young star clusters, Di Carlo et al. (2020) show that an additional 4% of BHs with masses larger than $60\,M_\odot$ form in models with lower metallicities ($Z \leqslant 0.002$ instead of $Z \leqslant 0.02$). On the other hand, at very high metallicities, increased stellar wind mass loss may inhibit the growth of massive black holes (e.g., Shrivastava & Kremer 2022). Thus, it would be interesting to expand this study to a wider range of metallicities. Additionally, GCs show evidence of multiple stellar populations, indicating that the properties of primordial binaries may be affected by complex gas-rich environments. Recent studies (e.g., Rozner & Perets 2022) have looked into the evolution of these systems and the repercussions on BBH merger rates.

As the recoil kicks are sensitive to spin magnitudes, our assumption of zero BH natal spin may be influencing the number of ejected BHs. Indeed, Rodriguez et al. (2019) showed that the number of 2G BBH mergers in dense star clusters decreases if a nonzero BH natal spin is assumed. However, as most mergers involving IMBHs already have unequal mass ratios, this property, along with the very low escape speeds of these clusters, should impart GW kicks large enough to eject the IMBH from the cluster.

Future studies will explore the impact of the IMF shape, coupled with a high binary fraction for massive stars, on the collision rates and massive BH formation. Weatherford et al. (2021) showed that a top-heavy stellar IMF increases the number of BHs significantly and enhances the BBH merger rate. Thus, a grid that encompasses both of these parameters would reveal an interesting spread of clusters with distinct populations of BHs.

This work was supported by NSF grant AST-2108624 and NASA grant 80NSSC22K0722. G.F. and F.A.R. acknowledge support from NASA grant 80NSSC21K1722. K.K. is supported by an NSF Astronomy and Astrophysics Postdoctoral Fellowship under award AST-2001751. N.C.W. acknowledges support from the CIERA Riedel Family Graduate Fellowship. Support for M.Z. is provided by NASA through the NASA Hubble Fellowship grant HST-HF2-51474.001-A awarded by the Space Telescope Science Institute, which is operated by the Association of Universities for Research in Astronomy, Inc.,

under NASA contract NAS5-26555. This research was supported in part through the computational resources and staff contributions provided for the Quest high performance computing facility at Northwestern University, which is jointly supported by the Office of the Provost, the Office for Research, and Northwestern University Information Technology.

ORCID iDs

Elena González Prieto https://orcid.org/0000-0002-0933-6438
Kyle Kremer https://orcid.org/0000-0002-4086-3180
Giacomo Fragione https://orcid.org/0000-0002-7330-027X
Miguel A. S. Martinez https://orcid.org/0000-0001-5285-4735
Newlin C. Weatherford https://orcid.org/0000-0002-9660-9085
Michael Zevin https://orcid.org/0000-0002-0147-0835
Frederic A. Rasio https://orcid.org/0000-0002-7132-418X

References

Abbott, B. P., Abbott, R., Abbott, T. D., et al. 2016, PhRvL, 116, 061102
Abbott, R., Abbott, T. D., Abraham, S., et al. 2020, arXiv:2010.14527
Abbott, R., Abbott, T. D., Abraham, S., et al. 2021, PhRvD, 125, 101102
Antonini, F., Gieles, M., & Gualandris, A. 2019, MNRAS, 486, 5008
Bacon, D., Sigurdsson, S., & Davies, M. B. 1996, MNRAS, 281, 830
Ballone, A., Costa, G., Mapelli, M., & MacLeod, M. 2022, arXiv:2204.03493
Banerjee, S. 2021, MNRAS, 500, 3002
Banerjee, S. 2022, A&A, 665, A20
Banerjee, S., Belczynski, K., Fryer, C. L., et al. 2020, A&A, 639, A41
Belczynski, K. 2020, ApJL, 905, L15
Belczynski, K., Heger, A., Gladysz, W., et al. 2016, A&A, 594, A97
Belczynski, K., Klencki, J., Fields, C. E., et al. 2020, A&A, 636, A104
Bond, J. R., Arnett, W. D., & Carr, B. J. 1984, ApJ, 280, 825
Breivik, K., Coughlin, S., Zevin, M., et al. 2020, ApJ, 898, 71
Bromm, V., & Larson, R. B. 2004, ARA&A, 42, 79
Campanelli, M., Lousto, C., Zlochower, Y., & Merritt, D. 2007, ApJL, 659, L5
Carr, B., Kühnel, F., & Sandstad, M. 2016, PhRvD, 94, 083504
Chatterjee, S., Fregeau, J. M., Umbreit, S., & Rasio, F. A. 2010, ApJ, 719, 915
Chatterjee, S., Rodriguez, C. L., & Rasio, F. A. 2017, ApJ, 834, 68
Chatterjee, S., Umbreit, S., Fregeau, J. M., & Rasio, F. A. 2013, MNRAS, 429, 2881
Chen, J.-H., & Shen, R.-F. 2018, ApJ, 867, 20
Costa, G., Ballone, A., Mapelli, M., & Bressan, A. 2022, MNRAS, 516, 1072
Costa, G., Bressan, A., Mapelli, M., et al. 2021, MNRAS, 501, 4514
Davies, M. B., Coleman Miller, M., & Bellovary, J. M. 2011, ApJL, 740, L42
Decarli, R., Walter, F., Venemans, B. P., et al. 2018, ApJ, 854, 97
Di Carlo, U. N., Giacobbo, N., Mapelli, M., et al. 2019, MNRAS, 487, 2947
Di Carlo, U. N., Mapelli, M., Giacobbo, N., et al. 2020, MNRAS, 498, 495
Di Carlo, U. N., Mapelli, M., Pasquato, M., et al. 2021, MNRAS, 507, 5132
Duquennoy, A., & Mayor, M. 1991, A&A, 248, 485
El-Badry, K., Quataert, E., Weisz, D. R., Choksi, N., & Boylan-Kolchin, M. 2018, MNRAS, 482, 4528
Fan, X., Strauss, M. A., Richards, G. T., et al. 2006, AJ, 131, 1203
Farmer, R., Renzo, M., de Mink, S. E., Fishbach, M., & Justham, S. 2020, ApJL, 902, L36
Farmer, R., Renzo, M., de Mink, S. E., Marchant, P., & Justham, S. 2019, ApJ, 887, 53
Fowler, W. A., & Hoyle, F. 1964, ApJS, 9, 201
Fragione, G., & Kocsis, B. 2018, PhRvL, 121, 161103
Fragione, G., Kocsis, B., Rasio, F. A., & Silk, J. 2022, ApJ, 927, 231
Fragione, G., Loeb, A., & Rasio, F. A. 2020, ApJL, 902, L26
Fragione, G., & Silk, J. 2020, MNRAS, 498, 4591
Fregeau, J. M., Ivanova, N., & Rasio, F. A. 2009, ApJ, 707, 1533
Fregeau, J. M., & Rasio, F. A. 2007, ApJ, 658, 1047
Fuller, J., & Ma, L. 2019, ApJL, 881, L1
Fuller, J., Piro, A. L., & Jermyn, A. S. 2019, MNRAS, 485, 3661
Gaburov, E., Lombardi, J. C. J., & Portegies Zwart, S. 2010, MNRAS, 402, 105
Gerosa, D., & Berti, E. 2019, PhRvD, 100, 041301
Giacobbo, N., & Mapelli, M. 2018, MNRAS, 480, 2011
Giersz, M., Leigh, N., Hypki, A., Lützgendorf, N., & Askar, A. 2015, MNRAS, 454, 3150
Giersz, M., Leigh, N., Marks, M., Hypki, A., & Askar, A. 2014, arXiv:1411.7603
Giesers, B., Kamann, S., Dreizler, S., et al. 2019, A&A, 632, A3
González, E., Kremer, K., Chatterjee, S., et al. 2021, ApJL, 908, L29
Gurkan, M. A., Fregeau, J. M., & Rasio, F. A. 2006, ApJL, 640, L39
Heger, A., & Woosley, S. E. 2002, ApJ, 567, 532
Heggie, D., & Hut, P. 2003, The Gravitational Million-Body Problem: A Multidisciplinary Approach to Star Cluster Dynamics (Cambridge: Cambridge Univ. Press)
Heggie, D. C. 1975, MNRAS, 173, 729
Hirano, S., & Bromm, V. 2017, MNRAS, 470, 898
Hopkins, A. M., & Beacom, J. F. 2006, ApJ, 651, 142
Inayoshi, K., Visbal, E., & Haiman, Z. 2020, ARA&A, 58, 27
Ivanova, N., Belczynski, K., Fregeau, J. M., & Rasio, F. A. 2005, MNRAS, 358, 572
Joshi, K. J., Rasio, F. A., & Portegies Zwart, S. 2000, ApJ, 540, 969
Kamann, S., Bastian, N., Usher, C., Cabrera-Ziri, I., & Saracino, S. 2021, MNRAS, 508, 2302
Katz, H., Sijacki, D., & Haehnelt, M. G. 2015, MNRAS, 451, 2352
Kimura, K., Hosokawa, T., & Sugimura, K. 2021, ApJ, 911, 52
Kremer, K., Lombardi, J. C. J., Lu, W., Piro, A. L., & Rasio, F. A. 2022, ApJ, 933, 203
Kremer, K., Spera, M., Becker, D., et al. 2020a, ApJ, 903, 45
Kremer, K., Ye, C. S., Rui, N. Z., et al. 2020b, ApJS, 247, 48
Kroupa, P. 2001, MNRAS, 322, 231
Kroupa, P., Subr, L., Jerabkova, T., & Wang, L. 2020, MNRAS, 498, 5652
Lada, C. J., & Lada, E. A. 2003, ARA&A, 41, 57
Limongi, M., & Chieffi, A. 2018, ApJS, 237, 13
Loeb, A., & Rasio, F. A. 1994, ApJ, 432, 52
Lousto, C. O., & Zlochower, Y. 2008, PhRvD, 77, 044028
Ma, L., Hopkins, P. F., Ma, X., et al. 2021, MNRAS, 508, 1973
Madau, P., & Rees, M. J. 2001, ApJL, 551, L27
Mahapatra, P., Gupta, A., Favata, M., Arun, K. G., & Sathyaprakash, B. S. 2021, ApJL, 918, L31
Maliszewski, K., Giersz, M., Gondek-Rosińska, D., Askar, A., & Hypki, A. 2022, MNRAS, 514, 5879
Mapelli, M. 2016, MNRAS, 459, 3432
Mapelli, M., Bouffanais, Y., Santoliquido, F., Arca Sedda, M., & Artale, M. C. 2022, MNRAS, 511, 5797
Mapelli, M., Spera, M., Montanari, E., et al. 2020, ApJ, 888, 76
Marchant, P., Renzo, M., Farmer, R., et al. 2019, ApJ, 882, 36
Mayer, L., Kazantzidis, S., Escala, A., & Callegari, S. 2010, Natur, 466, 1082
McKernan, B., Ford, K. E. S., Lyra, W., & Perets, H. B. 2012, MNRAS, 425, 460
Merritt, D., Milosavljević, M., Favata, M., Hughes, S. A., & Holz, D. E. 2004, ApJL, 607, L9
Miller, M. C., & Hamilton, D. P. 2002, MNRAS, 330, 232
Milone, A. P., Piotto, G., Bedin, L. R., et al. 2012, A&A, 540, A16
Moe, M., & Di Stefano, R. 2017, ApJS, 230, 15
Ober, W. W., El Eid, M. F., & Fricke, K. J. 1983, A&A, 119, 61
Oh, S. P., & Haiman, Z. 2002, ApJ, 569, 558
O'Leary, R. M., Kocsis, B., & Loeb, A. 2009, MNRAS, 395, 2127
Pattabiraman, B., Umbreit, S., Liao, W.-k., et al. 2013, ApJS, 204, 15
Peters, P. C. 1964, PhRv, 136, 1224
Pfister, H., Volonteri, M., Dubois, Y., Dotti, M., & Colpi, M. 2019, MNRAS, 486, 101
Portegies Zwart, S. F., Baumgardt, H., Hut, P., Makino, J., & McMillan, S. L. W. 2004, Natur, 428, 724
Portegies Zwart, S. F., & McMillan, S. L. W. 2002, ApJ, 576, 899
Ramirez-Ruiz, E., & Rosswog, S. 2009, ApJL, 697, L77
Renzo, M., Farmer, R. J., Justham, S., et al. 2020, MNRAS, 493, 4333
Rizzuto, F. P., Naab, T., Spurzem, R., et al. 2021, MNRAS, 501, 5257
Rizzuto, F. P., Naab, T., Spurzem, R., et al. 2022, MNRAS, 512, 884
Rodriguez, C. L., Amaro-Seoane, P., Chatterjee, S., et al. 2018, PhRvD, 98, 123005
Rodriguez, C. L., Chatterjee, S., & Rasio, F. A. 2016, PhRvD, 93, 084029
Rodriguez, C. L., & Loeb, A. 2018, ApJL, 866, L5
Rodriguez, C. L., Morscher, M., Pattabiraman, B., et al. 2015, PhRv, 115, 051101
Rodriguez, C. L., Weatherford, N. C., Coughlin, S. C., et al. 2022, ApJS, 258, 22
Rodriguez, C. L., Zevin, M., Amaro-Seoane, P., et al. 2019, PhRvD, 100, 043027
Rose, S. C., Naoz, S., Sari, R., & Linial, I. 2022, ApJL, 929, L22

Roupas, Z., & Kazanas, D. 2019, A&A, 632, L8
Rozner, M., & Perets, H. B. 2022, ApJ, 931, 149
Sana, H., de Mink, S. E., de Koter, A., et al. 2012, Sci, 337, 444
Sana, H., Gosset, E., & Evans, C. J. 2009, MNRAS, 400, 1479
Shrivastava, R., & Kremer, K. 2022, RNAAS, 6, 157
Spera, M., & Mapelli, M. 2017, MNRAS, 470, 4739
Spera, M., Mapelli, M., Giacobbo, N., et al. 2019, MNRAS, 485, 889
Stacy, A., Greif, T. H., & Bromm, V. 2012, MNRAS, 422, 290
Stevenson, S., Sampson, M., Powell, J., et al. 2019, ApJ, 882, 121
Tagawa, H., Haiman, Z., & Kocsis, B. 2020, ApJ, 892, 36
Takahashi, K., Yoshida, T., & Umeda, H. 2018, ApJ, 857, 111
The LIGO Scientific Collaboration, the Virgo Collaboration, Abbott, R., et al. 2021a, PhysRevD, 103, 122002
The LIGO Scientific Collaboration, the Virgo Collaboration, Abbott, R., et al. 2021b, ApJ, 915, 86
The LIGO Scientific Collaboration, the Virgo Collaboration, Abbott, R., et al. 2021c, ApJL, 913, L7
The LIGO Scientific Collaboration, the Virgo Collaboration, the KAGRA Collaboration, et al. 2021d, arXiv:2111.03634
Umbreit, S., Fregeau, J. M., Chatterjee, S., & Rasio, F. A. 2012, ApJ, 750, 31
Weatherford, N. C., Fragione, G., Kremer, K., et al. 2021, ApJL, 907, L25
Woosley, S. E. 2017, ApJ, 836, 244
Woosley, S. E. 2019, ApJ, 878, 49
Zevin, M., & Holz, D. E. 2022, ApJL, 935, L20
Zwart, S. F. P., & McMillan, S. L. W. 2002, ApJ, 576, 899